PHYSICAL REVIEW B **87**, 121104(R) (2013)

Terahertz quantum Hall effect of Dirac fermions in a topological insulator

A. M. Shuvaev,[1] G. V. Astakhov,[2] G. Tkachov,[3] C. Brüne,[4] H. Buhmann,[4] L. W. Molenkamp,[4] and A. Pimenov[1]

[1]*Institute of Solid State Physics, Vienna University of Technology, 1040 Vienna, Austria*

[2]*Physikalisches Institut (EP6), Universität Würzburg, 97074 Würzburg, Germany*

[3]*Institut für Theoretische Physik und Astronomie, Universität Würzburg, 97074 Würzburg, Germany*

[4]*Physikalisches Institut (EP3), Universität Würzburg, 97074 Würzburg, Germany*

(Received 9 August 2012; revised manuscript received 11 February 2013; published 14 March 2013)

Using terahertz spectroscopy in external magnetic fields, we investigate the low-temperature charge dynamics of strained HgTe, a three-dimensional topological insulator. In resonator experiments, we observe quantum Hall oscillations at terahertz frequencies, which offer direct access to the unusual electrodynamic properties of the surface states of topological insulators. The 2D density estimated from the period of the quantum Hall oscillations agrees well with dc transport experiments on the topological surface state. The Dirac character of the surface state is further evidenced by the observation of the characteristic Berry phase in the dependence of the Landau levels on magnetic field.

DOI: 10.1103/PhysRevB.87.121104 PACS number(s): 78.20.Ls, 73.43.−f, 78.20.Ek, 78.66.Hf

Three-dimensional topological insulators[1,2] have attracted much interest recently, as they exhibit a number of unusual and nontrivial properties, such as protected conducting states on the surfaces of the sample. Unusual electrodynamics, such as a universal Faraday effect and an anomalous Kerr rotation have been predicted[3–6] for these surface states, and their observation is still outstanding. We have shown recently that strained HgTe, where the strain lifts the light-hole–heavy-hole degeneracy that normally is present in bulk HgTe, is a very promising 3D topological insulator.[7] This is because at low-temperatures parasitic effects due to bulk carriers are practically absent. In static transport experiments, a strained 70 nm thick HgTe layer[7] exhibits a quantum Hall effect (QHE), yielding direct evidence that the charge carriers in these layers are confined to the topological two-dimensional (2D) surface states of the material. These findings are further corroborated by recent Faraday rotation data[8] in a similar layer, which have been obtained using a terahertz time-domain technique.

In this work, we report the first indication of the unusual electrodynamics of topological insulators. We observed quantum Hall effect induced oscillations in the terahertz response of a 52-nm-thick HgTe film at high magnetic fields.

The sample studied in this work is a coherently strained 52-nm-thick nominally undoped HgTe layer, grown by molecular beam epitaxy on an insulating CdTe substrate.[9] Transmittance experiments at terahertz frequencies (100 GHz $< \nu <$ 800 GHz) have been carried out in a Mach-Zehnder interferometer arrangement,[10,11] which allows measurement of the amplitude and phase shift of the electromagnetic radiation in a geometry with controlled polarization. Using wire grid polarizers, the complex transmission coefficient can be measured both in parallel and crossed polarizers geometry. Static magnetic fields, up to 8 Tesla, have been applied to the sample using a split-coil superconducting magnet.

To interpret the experimental data, we use the ac conductivity tensor $\hat{\sigma}(\omega)$ obtained in the classical (Drude) limit from the Kubo conductivity of topological surface states (see, e.g., Refs. 4 and 6). The diagonal $\sigma_{xx}(\omega)$ and Hall $\sigma_{xy}(\omega)$ components of the conductivity tensor as functions of terahertz frequency ω can be written as

$$\sigma_{xx}(\omega) = \sigma_{yy}(\omega) = \frac{1 - i\omega\tau}{(1 - i\omega\tau)^2 + (\Omega_c\tau)^2}\sigma_0, \quad (1)$$

$$\sigma_{xy}(\omega) = -\sigma_{yx}(\omega) = \frac{\Omega_c\tau}{(1 - i\omega\tau)^2 + (\Omega_c\tau)^2}\sigma_0. \quad (2)$$

Here, $\Omega_c = eBv_F/\hbar k_F$ is the cyclotron frequency, σ_0 is the dc conductivity, B is the magnetic field, v_F, k_F, e, and τ are the Fermi velocity, Fermi wave number, charge, and scattering time of the carriers, respectively. For the Dirac spin-helical surface states, the Fermi wave number depends on the 2D carrier density, n_{2D}, through the relation $k_F = \sqrt{4\pi n_{2D}}$, with no spin degeneracy.

The transmission spectra can then be calculated using a transfer matrix formalism,[12–14] which takes multiple reflection within the substrate into account. The electrodynamic properties of the CdTe substrate have been obtained in a separate experiment on a bare substrate. Further details of the fitting procedure can be found in the Supplemental Material to Ref. 14. Neglecting any substrate effects, the complex transmission coefficients in parallel (t_p) and crossed (t_c) polarizers geometry can be written as

$$t_p = \frac{4 + 2\Sigma_{xx}}{4 + 4\Sigma_{xx} + \Sigma_{xx}^2 + \Sigma_{xy}^2}, \quad (3)$$

$$t_c = \frac{2\Sigma_{xy}}{4 + 4\Sigma_{xx} + \Sigma_{xx}^2 + \Sigma_{xy}^2}. \quad (4)$$

Here, Σ_{xx} and Σ_{xy} are effective dimensionless 2D conductivities, defined as $\Sigma_{xx} = \sigma_{xx}dZ_0$ and $\Sigma_{xy} = \sigma_{xy}dZ_0$ with the HgTe film thickness $d = 52$ nm and the vacuum impedance $Z_0 \approx 377\ \Omega$. In order to self-consistently obtain the parameters of the quasiparticles, the field-dependent complex transmission $t_p(B)$ and $t_c(B)$ for $\nu = 0.17$, 0.35, and 0.75 THz and the zero-field transmittance spectra $|t_p(\omega)|^2$ have been fitted simultaneously.

The inset in Fig. 1 shows the transmittance spectrum of the HgTe film at zero magnetic field. The characteristic oscillations in the spectrum, with a period of about 58 GHz, are due to Fabry-Pérot type interferences within the CdTe substrate. The absolute transmittance in the interference maxima is

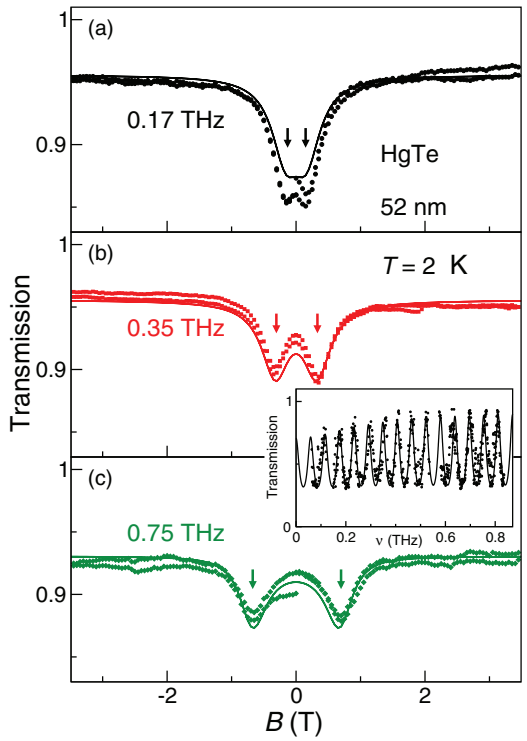

FIG. 1. (Color online) Magnetic field dependence of the transmission in strained HgTe. (a)–(c) Transmission amplitude in parallel polarizers (t_p) geometry, showing cyclotron resonance at the positions indicated by the arrows. The frequency of the experiments is indicated in the panels. The inset shows the frequency dependent transmittance in zero external magnetic field, $|t_p(B=0)|^2$. Symbols: experiment, solid lines: simultaneous fit of all data with the Drude model as described in the text.

close to 95%, which reflects the low effective conductance of our HgTe film, $\Sigma_{xx} \ll 1$. At low frequencies, the maximum transmittance decreases and approaches $|t_p|^2 \simeq 0.7$ in the zero frequency limit. Such a behavior is typical for Drude carriers with a scattering rate in the frequency region of the experiment. Indeed, the solid line in the transmission spectra represents a Drude fit with the parameters given in the first row of Table I.

From the fits, we obtain the Fermi velocity $v_F = 0.52 \times 10^6$ m/s. This value is very close both to $v_F = (0.51 \div 0.58) \times 10^6$ m/s as determined in the Faraday rotation experiments on a 70-nm-thick strained HgTe film[8] and to $v_F = 0.42 \times 10^6$ m/s as extracted from dc Shubnikov-de Haas measurements on a patterned 70-nm-thick strained HgTe layer.[7] The obtained value of the Fermi velocity is also in very good agreement with the band-structure-theory result $v_F = 0.51 \times 10^6$ m/s for the linear (Dirac) part of the surface-state spectrum in topological insulators (see, e.g., Ref. 15). As an additional check of the 2D surface carrier dynamics in our sample, we have analyzed the terahertz transmission data of Ref. 14 for a 70-nm-thick strained HgTe film at high temperature $T = 200$ K and for a bulk (1000-nm-thick) unstrained HgTe sample. In both cases, the electrodynamics is governed by massive bulk carriers, for which the values of v_F turn out to be much larger than the Dirac surface-state velocity, i.e., $v_F \approx 0.5 \times 10^6$ m/s (Table I).

Figure 1 shows the magnetic field dependent transmittance of the HgTe film in Faraday geometry and for parallel orientation of polarizer and analyzer. The experimental points for increasing and decreasing field do not fully coincide, which is most probably due to a magnetic hysteresis within the spectrometer. According to Eq. (3), the transmittance in parallel polarizers (t_p) depends mainly on Σ_{xx}. For all three frequencies two clear minima in the transmitted signal are observed in the range below ± 1 T. The minima in $|t_p|$ roughly correspond to the cyclotron resonance energy in HgTe[16] and scale with magnetic field. This may be understood taking into account that in our case $\Sigma \ll 1$ and Eqs. (3) and (4) simplify to

$$t_p \simeq 1 - \Sigma_{xx}/2, \quad t_c \simeq \Sigma_{xy}/2\,. \tag{5}$$

In the limit $\omega\tau \gg 1$, Eq. (1) may be approximated by

$$\sigma_{xx} \simeq \frac{1 - i\omega\tau}{\left(\Omega_c^2 - \omega^2\right)\tau^2}\sigma_0\,, \tag{6}$$

which leads to a resonance like feature for $\Omega_c = \omega$. Thus the positions and widths of the minima in Fig. 1 are directly connected with the parameter v_F/k_F and the scattering rate τ^{-1} of the charge carriers.

Figure 2 shows the complex Faraday angle $\theta + i\eta$ as obtained at the same frequencies as in Fig. 1. The polarization rotation θ and the ellipticity η are obtained from the transmission data using

$$\tan(2\theta) = 2\Re(\chi)/(1 - |\chi|^2)\,, \tag{7}$$

$$\sin(2\eta) = 2\Im(\chi)/(1 + |\chi|^2)\,. \tag{8}$$

Here, $\chi = t_c/t_p$ and the definitions of $\theta + i\eta$ are shown graphically in the inset to Fig. 2. A direct interpretation of the complex Faraday angle is, in general, not possible because of the interplay of σ_{xx} and σ_{xy} in the data.

In the low-frequency limit $\omega\tau \ll 1$, Eq. (2) simplifies to the static result $\sigma_{xy} = \Omega_c\tau\sigma_0/(1 + (\Omega_c\tau)^2)$. The last expression has a maximum at $\Omega_c(B) = \tau^{-1}$, which leads to maxima in t_c and θ at about the same field value. Therefore the Faraday

TABLE I. Drude parameters of the charge carriers in HgTe in strained and unstrained films. The data on 70-nm and 1000-nm films were partly given in Ref. 14.

Sample	T(K)	n_{2D}(cm^{-2})	v_F(ms^{-1})	$1/2\pi\tau$ (GHz)	$G_{2D} = \sigma_0 d$ (Ω^{-1})
52 nm (strained) [this work]	2	1.08×10^{11}	0.52×10^6	250	7.6×10^{-4}
70 nm (strained)[14]	4	4.8×10^{10}	0.38×10^6	210	4.3×10^{-4}
	200	1.5×10^{12}	1.63×10^6	360	5.3×10^{-3}
1000 nm (unstrained)[14]	3	4.2×10^{11}	0.99×10^6	240	2.8×10^{-3}
	200	4.9×10^{13}	9.36×10^6	360	1.9×10^{-1}

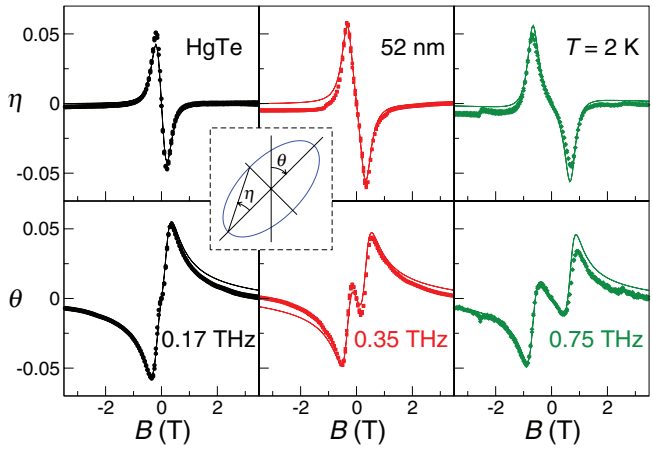

FIG. 2. (Color online) Complex Faraday angle $\theta + i\eta$ in HgTe. Bottom panels: Faraday rotation, top panels: ellipticity for the same frequencies as in Fig. 1. The inset sketches the definitions of the Faraday rotation θ and ellipticity η. Symbols: experiment, solid lines: simultaneous fit of *all* data using a single carrier response as described in the text. Angular units are radians.

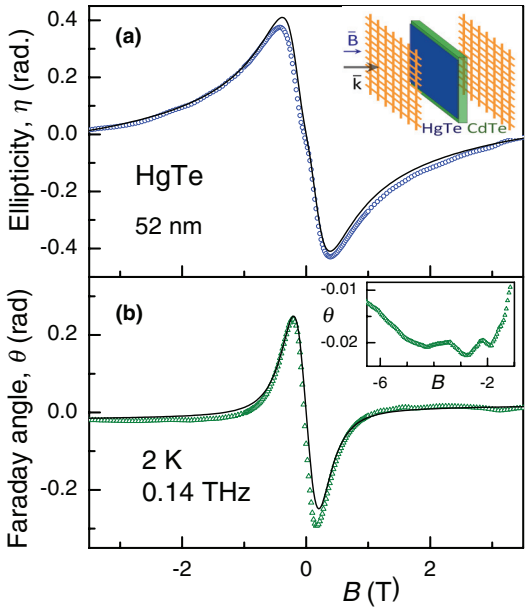

FIG. 3. (Color online) Faraday rotation in HgTe within resonator geometry. (a) Ellipticity and (b) Faraday angle. Symbols: experiment, lines, fits according to Eqs. (1)–(4). Upper inset shows the experimental geometry within a Copper meshes resonator. Lower inset shows a magnified view of the Faraday angle demonstrating QHE oscillations.

angle provides a direct and an independent way of obtaining the scattering rate $1/\tau$. The solid lines in Fig. 2 are the fits that have been done simultaneously for all results presented above. In total, the parameters of the charge carriers have been obtained by simultaneously fitting ten data sets. The quite reasonable fit of all results proves that a single type of charge carriers dominates the electrodynamics in the range of frequencies and magnetic fields used in these experiments.

Very solid evidence for the two-dimensional character of the carriers probed in the Faraday rotation experiments would be the observation of quantum Hall plateaus, similar to the observation of the QHE in Ref. 7. However, the accuracy of the experiments shown above does not allow to observe the QHE. In order to solve this problem, we have performed further Faraday transmission experiments on the same sample, now using a resonator geometry as shown in the inset of Fig. 3.

In these experiments, the sample is placed in the middle of a Fabry-Pérot resonator defined by metallic meshes. We have utilized Cu meshes with a 200-μm period. The distance between adjacent maxima of the resonator is $\simeq$51 GHz. In the frequency range between 100 and 200 GHz, the quality factor of the loaded resonator is about $Q \sim 10$. This indicates that, effectively, the radiation passes about ten times through the sample before reaching the detector, which effectively increases the sensitivity to fine details by roughly the same value. As shown in Fig. 3, in the resonator experiments the field dependence of the Faraday rotation and the ellipticity appears qualitatively similar to that in Fig. 2. An exact calculation of the complex transmission coefficients within a resonator is complicated because of the increased number of parameters. Therefore, in this case, we utilize the simple Eqs. (3) and (4), which neglect the effect of the substrate and the resonator completely. Nevertheless, as clearly seen in Fig. 3, the fits based on the simplified expressions reproduce the experimental results reasonably well. Fitting of the signals for parallel and crossed polarizers yields within experimental accuracy the same parameters as in the experiments without a resonator. The only parameter which differs from the results without a resonator is the absolute value of the conductivity. This is of course expected, and results from multiple transmission in the resonator and the influence of the substrate.

The main advantage of the resonator experiments is a higher sensitivity to the details of the field-dependent transmission. In addition to an overall field dependence similar to that in Figs. 1 and 2, a tiny modulation of the signal can now be observed. To convert this modulation to a conventional presentation, we have inverted the transmittance curves into the 2D conductivity, using Eqs. (3) and (4). Because the absolute transmittance is not well-defined in the resonator experiments, we have scaled the absolute 2D conductance to agree with the data without a resonator. The final results expressed in form of the effective 2D conductance $G_{xx,xy} = \Sigma_{xx,xy}/Z_0$ are shown in Fig. 4.

Figure 4(a) shows the real part of the two-dimensional conductance G_{xx} as a function of inverse magnetic field. Clear oscillations in the conductance can be observed in this presentation. Importantly, in Fig. 4(b) the oscillations in the Hall conductance are observed, showing a quantum Hall effect (QHE). In general, the phenomenology of the QHE at terahertz frequencies is not well understood.[17,18] Existing experiments have been limited to frequencies below 100 GHz and they are analyzed using scaling exponents.[17,19] The physics of the problem especially in topological insulators is still unexplored, because the frequency of the experiment is comparable to the cyclotron resonance and to the distance between the Landau levels in these materials. In present resonator experiments, the field dependent oscillations can be observed both with parallel and crossed polarizers. Contrary to G_{xx}, the off-diagonal conductance G_{xy} shows a substantial field dependence even in high magnetic fields. Therefore the

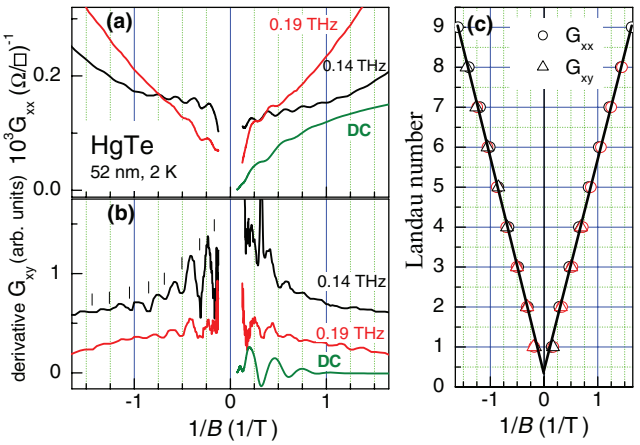

FIG. 4. (Color online) Terahertz quantum Hall effect in HgTe. (a) Two-dimensional conductance G_{xx}, and (b) the derivative of G_{xy} (dG_{xy}/dB^{-1}). The data have been obtained within a resonator geometry and are plotted as a function of inverse magnetic field. The experimental data are shown as solid lines for frequencies as indicated. Dashes in the bottom panel mark the minima for negative magnetic fields. (c) Numbered positions of the minima in G_{xx} and in the derivative of G_{xy} for 0.14 and 0.19 THz, respectively. Straight lines yield interpolation to the origin.

QHE signal is masked by the overall dependence of G_{xy}. In order to extract the QHE information from these data, we have plotted the derivative of the G_{xy} as a function of an inverse magnetic field (dG_{xy}/dB^{-1}) in Fig. 4(b). The derivative has the advantage of being insensitive to any residual slowly varying signals, and, importantly, the expected steps in G_{xy} are transformed into the minima of the derivative. Finally, in order to analyze the quantum Hall effect, both the minima in G_{xx} and in the derivative of G_{xy} have been taken into account. In Figs. 4(a) and 4(b), the results at finite frequencies are compared with dc QHE on the same sample. The periodicity of the oscillations in the dc experiments is slightly different because of different carrier concentration at the sample surface, induced by exposure to photoresist and the presence of ohmic contacts. We note that in agreement with Eq. (5) the oscillations in G_{xx} and G_{xy} are to large extent independent of each other as they are obtained in orthogonal experiments.[20]

The main results of the QHE experiments are represented in Fig. 4(c) demonstrating an approximate equidistant positioning of all minima (labeled by number N) in inverse magnetic fields B^{-1} with the period of $\Delta B^{-1} = 0.18$ T^{-1}. This periodicity reflects the dependence of the number of the occupied Landau levels on B^{-1}. In a total, we detect the oscillations up to index number ± 10; also, the first oscillations with the Landau level index ± 1 are clearly observed in the data. From the periodicity of these oscillations, the effective 2D carrier density can be estimated according to the free electron expression $n_{2D} = e/(h\Delta B^{-1}) \simeq 1.4 \times 10^{11}$ cm^{-2}. This value agrees reasonably well with the density $n_{2D} = 1.08 \times 10^{11}$cm^{-2} obtained directly from fitting the transmittance and the Faraday rotation on the basis of the Drude model (see Table I). Therefore we may conclude that charge carriers that are responsible for the terahertz electrodynamics at low temperatures reveal 2D behavior.

To further characterize the electron system in our sample, we extrapolated the dependence $N(B^{-1})$ to the origin [see straight lines in Fig. 4(c)], which corresponds to the limit of very strong magnetic fields. At the origin, we find a finite value $N \approx 1/2$ instead of $N = 0$ as would be the case for the conventional QHE. Previously, similar extrapolated values were reported for graphene (see, e.g., Ref. 21), zero-gap HgTe quantum wells[22] and strained 70 nm-thick HgTe films[7], i.e., for materilas with 2D Dirac-like charge carriers encoding a nonzero Berry phase. We therefore believe that our teraherz QHE also indicates the 2D Dirac-like behavior. We note, that a deviation from half-integer Landau numbers has been suggested recently[23] for nonideal Dirac fermions.

It is a quite remarkable result of the present work that only a single modulation period is observed in Fig. 4. This probably indicates that either the HgTe-substrate or HgTe-vacuum surface is not conducting and, therefore, is not seen in QHE data. Further support of this statement is given by the spectra in Fig. 2, where the curves at all frequencies can be well fitted simultaneously using only a single carrier response. We observe no additional features in the spectra which would justify a second Drude term. An artificial addition of such a term would lead to the same electrodynamic parameters with only two densities added. We therefore suggest the explanation of the present data using a response of a single surface.

In conclusion, we have analyzed the terahertz Faraday rotation in a strained HgTe film. From these data all relevant parameters of the conductivity can be obtained. In addition, terahertz quantum Hall effect oscillations have been observed within the same experiment. Our observations confirm the Dirac character of the carriers in the terahertz experiments and offer an inroad to the unusual electrodynamic properties of topological insulators.

We thank E. M. Hankiewicz for valuable discussion. This work was supported by the German Research Foundation (SPP 1285, FOR 1162) the joint DFG-JST Forschergruppe on "Topological Electronics," the ERC-AG project "3-TOP," and the Austrian Science Funds (I815-N16).

[1] M. Z. Hasan and C. L. Kane, Rev. Mod. Phys. **82**, 3045 (2010).
[2] Xiao-Liang Qi, Taylor L. Hughes, and Shou-Cheng Zhang, Phys. Rev. B **78**, 195424 (2008).
[3] Wang-Kong Tse and A. H. MacDonald, Phys. Rev. Lett. **105**, 057401 (2010).
[4] Wang-Kong Tse and A. H. MacDonald, Phys. Rev. B **84**, 205327 (2011).
[5] Joseph Maciejko, Xiao-Liang Qi, H. Dennis Drew, and Shou-Cheng Zhang, Phys. Rev. Lett. **105**, 166803 (2010).
[6] G. Tkachov and E. M. Hankiewicz, Phys. Rev. B **84**, 035405 (2011).
[7] C. Brüne, C. X. Liu, E. G. Novik, E. M. Hankiewicz, H. Buhmann, Y. L. Chen, X. L. Qi, Z. X. Shen, S. C. Zhang, and L. W. Molenkamp, Phys. Rev. Lett. **106**, 126803 (2011).

[8] Jason N. Hancock, J. L. M. van Mechelen, Alexey B. Kuzmenko, Dirk van der Marel, Christoph Brüne, Elena G. Novik, Georgy V. Astakhov, Hartmut Buhmann, and Laurens W. Molenkamp, Phys. Rev. Lett. **107**, 136803 (2011).

[9] C. R. Becker, C. Brüne, M. Schäfer, A. Roth, H. Buhmann, and L. W. Molenkamp, Physica Status Solidi **4**, 3382 (2007).

[10] A. A. Volkov, Yu. G. Goncharov, G. V. Kozlov, S. P. Lebedev, and A. M. Prokhorov, Infrared Phys. **25**, 369 (1985).

[11] A. Pimenov, S. Tachos, T. Rudolf, A. Loidl, D. Schrupp, M. Sing, R. Claessen, and V. A. M. Brabers, Phys. Rev. B **72**, 035131 (2005).

[12] D. W. Berreman, J. Opt. Soc. Am. **62**, 502 (1972).

[13] A. M. Shuvaev, S. Engelbrecht, M. Wunderlich, A. Schneider, and A. Pimenov, Eur. Phys. J. B **79**, 163 (2011).

[14] A. M. Shuvaev, G. V. Astakhov, A. Pimenov, C. Brüne, H. Buhmann, and L. W. Molenkamp, Phys. Rev. Lett. **106**, 107404 (2011).

[15] C.-X. Liu, X.-L. Qi, H. J. Zhang, Xi Dai, Z. Fang, and S.-C. Zhang, Phys. Rev. B **82**, 045122 (2010).

[16] M. Zholudev, A. Ikonnikov, F. Teppe, M. Orlita, K. Maremyanin, K. Spirin, V. Gavrilenko, W. Knap, S. Dvoretskiy, and N. Mihailov, Nanoscale Res. Lett. **7**, 534 (2012).

[17] F. Hohls, U. Zeitler, R. J. Haug, R. Meisels, K. Dybko, and F. Kuchar, Phys. Rev. Lett. **89**, 276801 (2002).

[18] Y. Ikebe, T. Morimoto, R. Masutomi, T. Okamoto, H. Aoki, and R. Shimano, Phys. Rev. Lett. **104**, 256802 (2010).

[19] S. L. Sondhi, S. M. Girvin, J. P. Carini, and D. Shahar, Rev. Mod. Phys. **69**, 315 (1997).

[20] The leakage of σ_{xx} into σ_{xy} within the resonance condition have been estimated for Fabry-Pérot interferences within the substrate. For typical parameters of our film, the leakage $\frac{\partial \ln(t_p)/\partial \ln(\sigma_{xy})}{\partial \ln(t_p)/\partial \ln(\sigma_{xx})}$ is less than 0.1–0.15. Most importantly, the leakage $\frac{\partial \ln(t_c)/\partial \ln(\sigma_{xx})}{\partial \ln(t_c)/\partial \ln(\sigma_{xy})}$ is smaller than 10^{-3}–10^{-2} for magnetic fields above 1 T. The absolute value of the QHE modulation in σ_{xy} is about $\Delta\sigma_{xy}/\sigma_{xy} \sim 5$–10%.

[21] K. S. Novoselov, A. K. Geim, S. V. Morozov, D. Jiang, M. I. Katsnelson, I. V. Grigorieva, S. V. Dubonos, and A. A. Firsov, Nature (London) **438**, 197 (2005).

[22] B. Büttner, C. X. Liu, G. Tkachov, E. G. Novik, C. Brüne, H. Buhmann, E. M. Hankiewicz, P. Recher, B. Trauzettel, S. C. Zhang, and L. W. Molenkamp, Nat. Phys. **7**, 418 (2011).

[23] A. A. Taskin and Yoichi Ando, Phys. Rev. B **84**, 035301 (2011).